Perfluorinated Self-Assembled Monolayers enhance the Stability and Efficiency of Inverted Perovskite Solar Cells

Christian M. Wolff [A*], Laura Canil[Ba], Carolin Rehermann[Bc] , Nguyen Ngoc Linh[C], Fengshuo Zu[E,F], Maryline Ralaiarisoa[E], Pietro Caprioglio [A,Bb], Lukas Fiedler [A], Martin Stolterfoht[A], Sergio Kogikoski Jr.[A], Ilko Bald[A], Norbert Koch[E,F], Eva Unger[Bc,G], Thomas Dittrich[B], Antonio Abate[Ba,D *] and Dieter Neher [A*]

A. Universität Potsdam
Karl-Liebknecht-Str. 24-25
14776 Potsdam, Germany

B. Helmholtz-Zentrum Berlin für Materialien und Energie
Kekuléstraße 5
12489 Berlin, Germany
   a. Young Investigator Group Active Materials and Interfaces for Stable Perovskite Solar Cells
   b. Young Investigator Group Perovskite Tandem Solar Cells
   c. Young Investigator Group Hybrid Materials Formation and Scaling

C. Institute for Molecular Engineering
The University of Chicago, Chicago
Illinois 60637, USA

D. Department of Chemical, Materials and Production Engineering
University of Naples Federico II
Piazzale Tecchio 80, 80125 Fuorigrotta, Naples, Italy

E. Institut für Physik & IRIS Adlershof, Humboldt-Universität zu Berlin, 12489 Berlin, Germany

F. Helmholtz-Zentrum Berlin für Materialien und Energie GmbH, 12489 Berlin, Germany

G. Department of Chemistry and NanoLund, Lund University, 221 00 Lund, Sweden

KEYWORDS inverted perovskite solar cells, self-assembled monolayers, stability, interfaces, recombination

ABSTRACT: Perovskite solar cells are amongst the most exciting photovoltaic systems as they combine low recombination losses, ease of fabrication and high spectral tunability. The Achilles heel of this technology is the device stability due to the ionic nature of the perovskite crystal, rendering it highly hygroscopic, and the extensive diffusion of ions especially at elevated temperatures. Herein, we demonstrate the application of a simple solution-processed perfluorinated self-assembled monolayer (p-SAM) that not only passivates the perovskite surface but also drastically improves the stability of the perovskite absorber and in turn the solar cell under elevated temperature or humid conditions. p-i-n-type perovskite devices employing these SAMs exhibited power conversion efficiencies surpassing 21%. Notably, the best performing devices are stable under standardized maximum-power point (MPP) operation at 85°C in inert atmosphere (ISOS-L-2) for more than 250 h, and exhibit superior humidity resilience, maintaining ~95% device performance even if stored in humid air in the ambient over months (~3000h, ISOS-D-1). Our work, therefore, demonstrates a novel strategy towards efficient and stable perovskite solar cells with easily deposited functional interlayers.

Introduction

The last years have witnessed a huge improvement in the efficiency and stability of solar cells based on metal halide perovskites. Systematic improvements of the perovskite composition and morphology, combined with the development of new charge transporting materials led to certified power conversion efficiencies (PCEs) of up to 25.2 %.[1] In parallel, various strategies have been developed to improve the stability of the perovskite itself and the entire device and good-to-excellent stabilities in light, air or electrical load stress tests have been demonstrated.[2,3] Many of these approaches however required rather complicated and thus expensive encapsulation schemes, such as deposition of inorganic layers by ALD (atomic-layer-deposition) or sputtering.[4,5] A few early attempts include the use of long-alkyl chain halide molecules for surface modifications, other moisture repelling molecules[6] or the crosslinking agent ABPA[7]. Likewise, Lewis-base passivation protocols[8,9] have shown to improve the performance and stability, and recently composites incorporating 2D perovskites were shown to exhibit substantially improved resilience to environmental stress[10–13]. Notably, most of the recent achievements towards high efficiencies and/or stability employed n-i-p architecture, where the active perovskite is coated on a (commonly-used) n-type transparent metal oxide and the cell is completed with a fairly thick (and often doped) p-type organic semiconductor. To the best of our knowledge, the most stable (encapsulated) n-i-p devices were reported by Grancini & Roldán-Carmona et al.[11] (initial PCE: 12%, sealed and measured in ambient, 10.000h at J_{SC} at 55°C without loss), by Christians et al.[14] (initial PCE: 12.2%, measured in ambient (10-20%RH) for >1000h close to MPP at 30°C, retaining >88% efficiency), by Saliba et al.[15] (initial PCE: 17%, MPP-tracking in nitrogen for 500h at 85°C, retaining 95% efficiency) and by Jeon et al.[16] (initial PCE: 20.8%, encapsulated and measured in ambient at 25°C for 300h, retaining 92% efficiency). On the other hand, p-i-n cells are particularly attractive due to their very simple device architecture, often comprising very thin charge-transporting layers with the perovskite active layer occupying over 90% of the cell volume. These cells often use undoped organic charge transport layers and are processed at temperatures below 100°C. Chemical doping has been identified as one major source for device degradation[17]. Probably most importantly, p-i-n is the preferred architecture for tandem applications on p-type silicon such as "PERC" cells (which currently exhibit a market share of over 90% of all industrial solar cells). Therefore, and perhaps not surprisingly, all recently published record monolithic Si/perovskite tandem cells employed a p-i-n type cell on top of a p-type silicon cell[18–20]. Unfortunately, the efficiency and stability of p-i-n type cells lack behind those of the more commonly employed n-i-p architectures. In this context, it has been acknowledged that non-radiative recombination of photogenerated charges at the interface between the perovskite and the electron-transporting layer (ETL) is a major loss channel, especially in p-i-n devices. Various strategies (such as compositional engineering[21] or addition of interlayers[22–24]) have been demonstrated to reduce these losses, resulting in reproducible efficiencies of up to 20.9% for small devices and 19.8% on 1 cm^2 pixels. On the other hand, very few publications report long-term stabilities of p-i-n type cells under relevant storage or illumination conditions. For example Zheng et al. showed moderate stability of an unencapsulated cell under ambient MPP tracking for 25 h with high efficiencies[25], and we previously reported a stability of 168 h on a non-encapsulated cell with a PCE of 16% under MPP tracking at 25°C in inert gas[26]. A successful approach to improve the stability of p-i-n-type perovskite solar cells it to protect the active perovskite by combining an ALD-deposited transparent metal oxide layer in combination with e.g. sputtered top contacts or AZO-NPs, and these devices showed exceptional lifetimes (e.g. a T80 of 100 h during MPP at 100°C in ambient atmosphere for <16% PCE devices[27,28] or 1000 h in ambient MPP with an initial PCE of 13%[29]) Other approaches to increase the stabilities of such cells include silane molecules[30] or the use of quaternary ammonium halides to passivate the perovskite or multiple ALD layers[31]. With the above-mentioned exceptions, p-i-n devices are usually not subjected to simultaneous thermal-light-bias stress and no highly efficient (>20%) devices have been shown to rival the stability of the n-i-p structured devices.

In this report, we introduce a simple yet effective functionalization of a triple cation lead halide perovskite with a self-assembled monolayer (SAM) made of 6 to 12 carbon atoms perfluorinated aliphatic molecules terminated with an iodine or bromine-anchoring group. p-i-n cells comprising these layers exhibit efficiencies above 21% while being processed at temperatures no higher than 100°C. The layer significantly improves the resilience of the whole solar cell to heat, light or moisture. If operated at the maximum power point, the cells maintain 99% of their initial efficiency even after 250 h of continuous illumination at 85°C (ISOS-L-2 conditions). This is remarkable given that the chosen p-i-n structure is fully processed at low temperatures, doesn't require chemical dopants or any other encapsulation.[32–35]

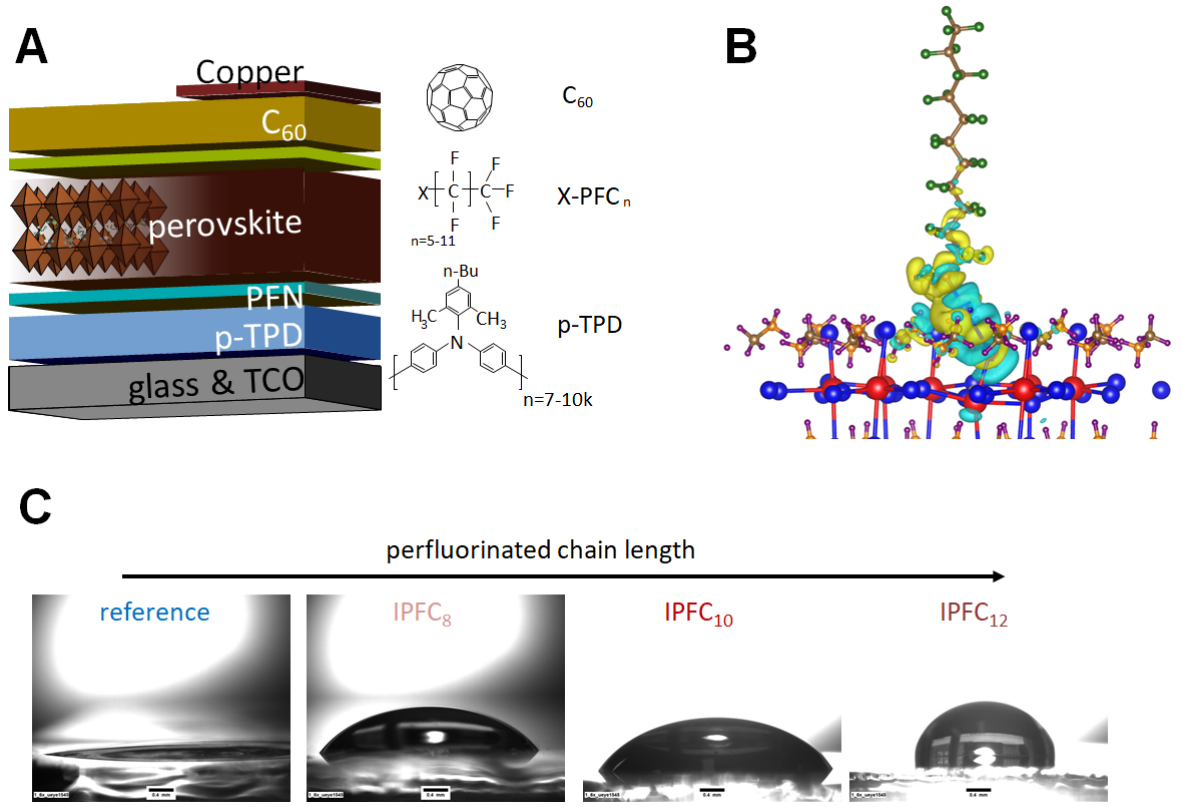

Figure 1. A) Schematics of the p-i-n-type device architecture showing the position of the individual layers, as well as the chemical structure of the molecules used for the SAM preparation and the transport layers. B) Density functional theory (DFT) simulations of the coupling between an I-PFC12 molecule and a perovskite (I-terminated) surface together with the positive (yellow) and negative (turquoise) charge redistribution responsible for the halogen-type bonding. C) Contact angle measurements of 2-propanol on perovskite|IPFCx-SAM-samples with different n= 0, 8, 10, 12.

Results

Device Performance

Figure 1 displays our standard p-i-n solar cell architecture with the structure ITO|HTL|$CsI_{0.05}[FA_{0.85}MA_{0.15}Pb(I_{0.85}Br_{0.15})_3]_{0.95}$|SAM|$C_{60}$|BCP|Cu. Such cells exhibit power conversion efficiencies of roughly 19% with an average open-circuit voltage of <1.1V, 77% fill -factor (FF) and a short-circuit current density (J_{SC}) of 2.3 mA/cm². The embedment of the p-SAMs directly influences all photovoltaic parameters, depending on the nature of the anchoring group (iodine or bromine) and the length of the perfluorinated carboxylic tail (Figure 2A). We deposit the SAMs by submerging the annealed perovskite for ~20 min. in a dilute solution of the respective molecules (10mM), which we found to be the optimum concentration in initial tests (Figure S2). Notably, the iodine-terminated molecules improve the photovoltaic performance, predominately through the improvement of V_{OC} to an average above 1.15V while other metrics remain practically unchanged. The current density of 22.5 $mAcm^{-2}$ is confirmed by the integrated EQE_{PV} spectrum in Figure S1. Employing a Br-terminated SAMs increases the V_{OC} above 1.10V but causes a continuous drop of the fill-factor (FF) with the increasing length of the perfluorinated tail, resulting in an overall reduction of the PCE. Given the fact that the nature of the binding moiety affects mainly the FF, we speculate that the drop in efficiency upon inserting the Br-terminated SAM is related to the efficiency of charge extraction. This point will be addressed later. The optimal performance in this series is obtained with I-PFC10 - perfluorodecyl iodide, where we achieve a V_{OC} of 1.18 V at a thermodynamic limit of 1.32 V. This is amongst the highest open-circuit voltage reported for p-i-n type perovskite solar cells – beaten only by a very recent approach using a secondary perovskite phase at the perovskite/ETL interface[21] or with very specific processing conditions and unstable transient behavior (i.e. strong light soaking required)[36]. The corresponding non-radiative loss in potential is only ~150 mV, which is amongst the lowest losses for the given bandgap of the absorber - irrespective of the architecture. As a result, inserting I-PFC10 causes an average improvement of the PCE by absolute 1.5%, with a record efficiency of 21.3% (average 20.5%). We note

that the devices do not exhibit pronounced hysteric effects, irrespective of scan speed or direction and the obtained efficiencies coincide with the stabilized MPP output (Figure 2(B, C) and Figure S3).

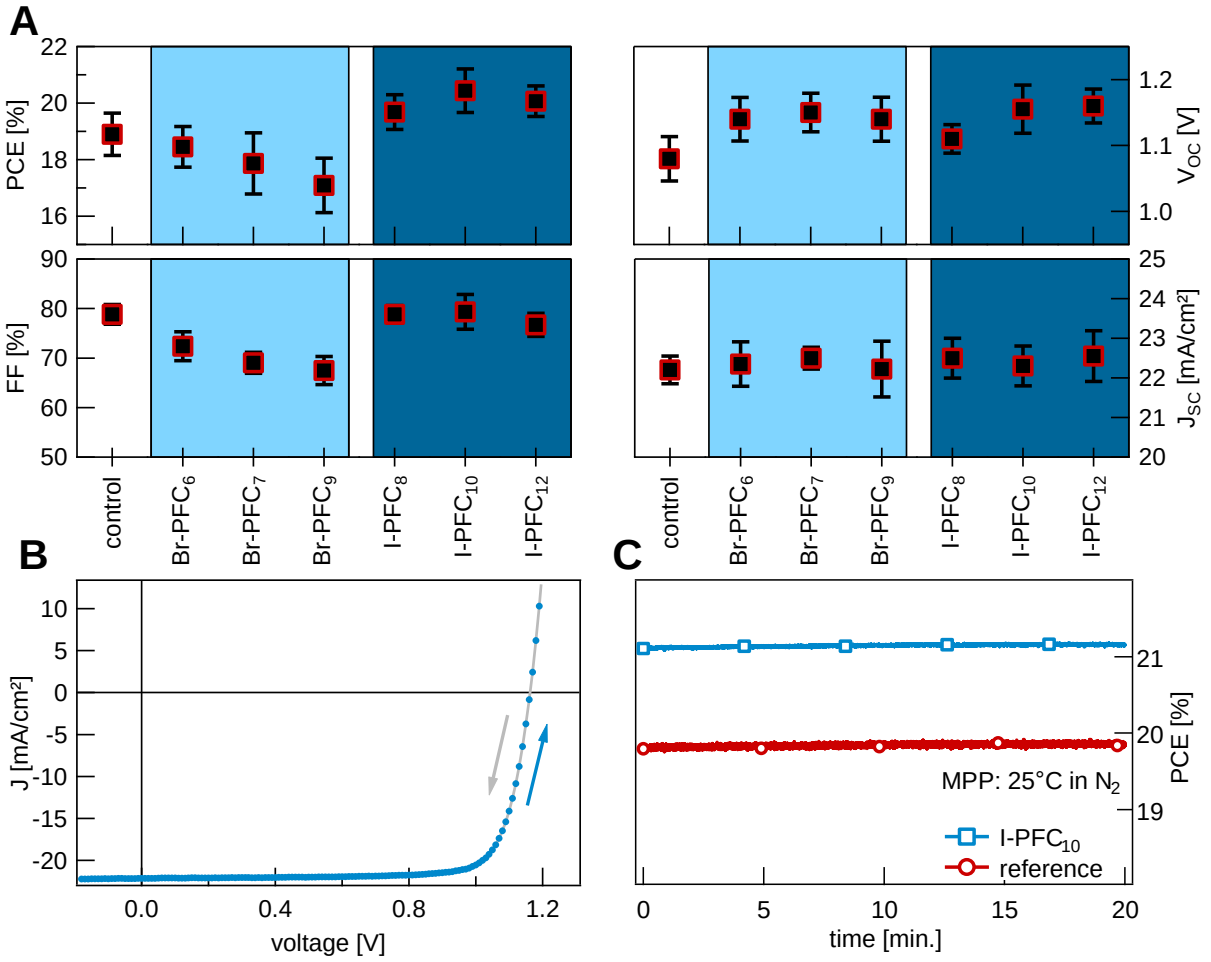

Figure 2. A) Average statistics of the photovoltaic parameters PCE, V_{OC}, FF and J_{SC} over several batches including the standard deviation of each parameter. B) JV-curve of the best performing device with an I-PFC10 SAM in forward and backward scan direction (100 mV/s), yielding a PCE of 21.3%. C) Representative maximum power point (MPP) tracking over the course of 20 minutes of one of the highest performing I-PFC10 and reference devices.

SAM bond formation and layer characteristics

It has been proposed that halogenated organic compounds bind to undercoordinated halide anions at the perovskite surface by the formation of noncovalent halogen bonds.[37] The binding and SAM properties of I-terminated perfluorocarbons on different model interfaces has been studied recently[38]. For I-PFC12 on silicon nitride, density functional theory (DFT)[38] revealed non-covalent halogen bond formation, where approximately 0.5 electrons were transferred from the nucleophilic nitrogen surface atom to the electrophilic iodine atom, going along with large binding energy of 128 kJ/mol. Halogen bond formation was confirmed by ssNMR on self-assembled monolayer adsorbed to SiNx nanoparticles. The study of a SAM on a flat SiN_x with X-ray reflectometry and contact angle measurements revealed the formation of a dense molecular with a critical surface energy of only 2.6 Nm.

DFT calculations were performed to explore the potential interaction of our SAM molecules to the perovskite surface. Since we were interested specifically in nature and strength of a possible binding of the SAM molecules to the halide anions, we restricted our simulations to the case that molecules adsorb on an I-terminated (111) perovskite surface (calculation details are given in the Supplementary Note 1). In Scheme S1, we show the side views of I-PFC12 molecules assembled on a perovskite surface.

Albeit these are simplifications - for example, the perovskite surface may expose different facets[39] - this DFT model is useful to elucidate the electron distribution at the hybrid interface and with that the strength and nature of a formed I-I bond. Similar to the case of I-PFC12 on silicon, silicon nitride or silicon oxide surface, the interaction between I-PFC12 and the perovskite surface is primarily

electrostatic in nature, although second order contributions such as polarization, dispersion, and charge transfer are present.[40] Figure 1B shows the iso-surface plot of the induced charge density, defined as $\Delta n(r) = n_{tot} - [n_{mol} + n_{surf}]$, i.e. the difference between the charge density of the adsorption system and the sum of the isolated I-PFC12 molecule and the perovskite surface. The Löwdin atomic charge analysis[41] of such molecule-substrate system reveals that up to 0.3 electrons to be transferred from the nucleophilic iodine surface to the electrophilic iodine atom of the molecule with respect to its neutral valence charge. The computed binding energy is 183 kJ/mol, higher than the binding energy between I-PFC12 on silicon nitride surface (128 kJ/mol).[40,42–45]

To confirm the existence of a SAM on our perovskite samples, we carried out photoemission (X-ray photoemission spectroscopy, Figure S4) and Fourier-transformed Infrared spectroscopy (FTIR, Figure S5) studies on neat and SAM-modified perovskite samples. The F1s core-level XPS spectra reveal the presence of fluorinated species on the surface of the perovskite concurrent with a shift in workfunction as obtained from Kelvin probe measurements (both Figure S4). Unfortunately, we were not able to deduce specific information on the type of binding from these XPS spectra. It is known that X-ray illumination and substrate-induced photochemical reactions may remove iodine from the molecules. FTIR spectra shown in Figure S5 consolidate the presence of the molecules on-top of the perovskite, as indicated by the appearance of additional modes at 1150-1300cm^{-1} - absent in the unmodified perovskite. Interestingly, we observed a small blue shift of the prominent molecular bands of the SAM (Figure S5C) at ~1200 and 1150cm^{-1}, when deposited on the perovskite. This may indicate a larger degree of disorder in the surface-bound molecular layer compared to the pristine I-PFC12. One reason for this may be the strong binding of the I-terminated molecule to the perovskite, as suggested by the above DFT calculations. Strong surface binding is known to inhibit the formation of dense molecular packing by reducing the mobility of the molecules along the surface. In fact, comparing the strength of the I3d5/2 signal of the pristine perovskite and a samples modified with a I-PFC10 revealed an average thickness of the I-terminated SAM of only 2.6 Å. This value may be considered as a lower limit due to the instability of the I-binding under X-ray exposure. Notably, the estimated average thickness of the Br-terminated SAM (in this case BrPFC9) is larger, ca. 4.7Å. Also, the comparison of the FTIR spectra of the surface-bound molecules and the dense molecular film revealed identical peak positions, indicative of a higher molecular ordered in the Br-terminated SAM. This may be due to a smaller strength of the formed halogen bond[46,47], rendering the Br-terminated molecules more mobile. The formation of a denser and thicker SAM from the Br-terminated perfluorocarbons may be the reason for the significant lowering of the FF with increasing molecular length and concentration as noted above[38,48,49].

Proof for a dense coverage of the perovskite surface with perfluorinated carbon chains (even in case of I-termination) comes from the measurements of contact angle. Figure 1C shows photographs of contact angle measurements with 2-propanol (IPA) on the perovskite with and without the iodated SAMs. The sample without any treatment shows a contact angle <5° which steadily rises when employ ying SAMs with longer tails, reaching 88° in the case of I-PFC12.

Loss in Potential and Improvement of the V_{OC}

The significant increase of the V_{OC} upon insertion of the SAMs requires special attention. It has previously been shown that any improvement in V_{OC} is related to an increase in bandgap or a reduction of recombination, either in the perovskite bulk, at the perovskites' surface or the interface with an adjacent layer.[23,50–54] In previous publications, we have identified interfacial recombination as the primary source for a reduced photovoltage of p-i-n-type perovskite solar cells[23,24]. Mitigating these losses often comes at the expense of a loss in fill-factor[23,55–57]. However, the exact origin of the V_{OC} improvements will depend largely on the system of interest, and it is yet not clear whether additives or interlayers improve V_{OC} by reducing recombination in the bulk (and grain boundaries) or at the interfaces with the adjacent transport layers[58].

It has been proposed that the binding of organohalides to a perovskite surface reduces the density of surface traps[37]. To investigate whether our SAMs improve the V_{OC} predominantly via trap passivation or through the suppression of interfacial recombination, we determined the quasi-Fermi-level splitting (QFLS) in the perovskite through the measurement of the absolute PL on the neat perovskite, multilayer stacks or on full devices through[59]:

$$QFLS = k_B T \times \ln\left(PLQY \times J_G / J_{0,rad} + 1\right) \quad (1)$$

Here, PLQY is the external quantum efficiency of photoluminescence, and J_G/q and $J_{o,rad}/q$ is the photon flux of solar and black body radiation, respectively, which is absorbed/emitted by the active layer. Note that Equation (1) is only correct in absence of exciton effects, meaning that every absorbed photon generates an electron-hole pair and that all PL stems from direct free carrier recombination. As the QFLS in the absorber limits the V_{OC} of the solar cell, information on the QLFS and how it is affected by the placement of the SAM and the addition of the charge-transporting layers is of crucial importance for the understanding of the V_{OC} improvement.

For the pure absorber or the absorber in contact with additional layers under the condition of no electrical contact any charges generated in the device must recombine within this stack. In the ideal case, all absorbed photons are simply reemitted – called photoluminescence. In addition to photon emission, the electrons and holes can also lose their energy through non-radiative electron-phonon coupling[60] resulting in the dissipation of heat, which would reduce PLQY, reducing the QFLS.[61] Thus, measuring the rate of emitted photons versus generated carriers is a measure of how energy is lost through these unwanted processes. We performed several pulsed and steady-state measurements to unambiguously show the processes that limit the solar cells' V_{OC}'s at varying carrier densities. In Figure 3A, we show the EQE_{PV} spectra of the perovskite solar cells measured under short circuit conditions. All devices exhibit a very similar spectral shape with a bandgap of 1.61 eV (half-maximum) and Urbach energies of ~ 15 meV. The deduced generation ($J_G=J_{SC}= \int \Phi_{sun} \cdot EQE_{PV}\, dE$) and minimal recombination current at 300 °K ($J_{o,rad.}= \int \Phi_{BB} \cdot EQE_{PV}\, dE$) are ~22 mA cm^{-2} (see Figure S1) and ~3 x 10^{-21} mA cm^{-2}, respectively. Here, we also assume that all photogenerated charge carriers reach the electrodes under short circuit conditions, which is a reasonable assumption given that perovskite solar cells with comparable bandgap show flat internal quantum efficiency spectra with close to 100% efficiency. This results in a radiative limit of 1.34 eV for the obtainable QFLS and thus V_{OC} (details on the calculations are in Supplementary Note 2)[52,62–64]. As the devices' V_{OC}'s are substantially lower than that, we obviously suffer from substantial additional recombination currents. In order to decouple the losses, we measured the luminescent efficiency of samples that are made from the individual layers (always with perovskite) of the solar cell stack or of the whole solar cells. Figure 3B and Figure S3 show the obtained PL spectra of four samples at 1-sun equivalent illumination conditions. The pristine perovskite has an external PLQY of just below 1%, which allows for a maximum QFLS of 1.23 eV (see Supplementary Note 2).Adding the SAMs to the neat perovskite film has no effect on the PL emission properties (Figure S6), irrespective of the nature of the anchoring group used herein. Therefore we can rule out surface passivation of device-relevant traps as the main source for the significant improvement of the device performance. On the other hand, the perovskite in direct contact with C_{60} only emits 1 photon for every ~10^5 incoming photons (Figure 3B). Upon introduction of the perfluorinated SAMs this reduction is mitigated by almost two orders of magnitude rendering PLQYs of ~0.5% This implies, that the non-radiative losses at this interface are reduced by up to $k_B T \cdot ln\left(\frac{10^{-5}}{10^{-3}}\right) \approx 120 meV$, comparable to the average improvement in the device V_{OC} of ~ 90 mV (105 mV in the best case). These experiments were complemented by the investigation of the carrier dynamics after photogeneration by performing time-resolved photoluminescence (tr-PL) measurements at low excitation intensities. This allows deducing mean carrier lifetimes free of capacitive effects,[65] which in turn yield the average carrier densities under steady-state illumination in the limit of predominant first-order recombination from which VOC can be estimated (see Supplementary Note 2)[64]. The pure perovskite has PL decay times (1/e) of ~600-800 ns. Plugging this into Equations S5 and S6 results in a QFLS of up to 1.23eV, consistent with the previous PLQY measurements. We note again that this is to be expected, only, if the transient PL decay is dominated by a first-order recombination loss, e.g. recombination via traps in the bulk or by interfacial recombination, while free carrier recombination is insignificant[66]. Importantly, as shown in Figure 3b, the functionalization of the perovskite with the SAMs (but without the presence of C_{60}) did not change the monoexponential tr-PL lifetime, again ruling out trap passivation as the source of the improvement in VOC, which is also evident from the absolute PL measurements on pristine vs. modified perovskite as noted above In contrast, depositing C_{60} on the perovskite reduces the lifetime dramatically. Albeit it has been suggested that fullerenes passivate traps in the perovskite or rather at the grain boundaries[67,68], we observe a drastic reduction of carrier lifetime, which is consistent with the large decrease in QFLS as noted above. The carrier lifetime can be however partially recuperated by interjecting SAMs. The lifetimes rise from ~25 ns (C_{60} only) up to ~150 ns, which allow us to calculate obtainable QFLS's of 1.080 eV and 1.173 eV, respectively, in excellent agreement to the measured V_{OC}'s. Finally, we combined measurements of the EQE_{PV} and of the external quantum efficiency of electroluminescence, EQE_{EL}, on

full devices to deduce values of V_{OC} with Rau's reciprocity relation. In contrast to the methods described above, Rau's reciprocity explicitly considers the exchange of charges between the perovskite absorber to the contacts. It has been pointed out before that errors between the predicted and measured V_{OC} may arise from insufficient collection and/or injection of charges.[69] Figure 3D summarizes the results from all three techniques on multiple samples. We supported these findings by measuring the surface-photovoltage (SPV) on half-cells comprising ITO|HTL|perovskite alone, or capped with C_{60}, the SAMs or SAMs and C_{60}. The spectrally dependent voltage build-up (photovoltage) of the devices (Figure S7C) without C_{60} exhibits no appreciable difference between pristine or modified perovskites, indicating that the electronic structure of the perovskite at the surface is not changed. Yet, with the C_{60} present (Figure S7B), the situation differs, as the samples are now able to separate charges (i.e. generate voltage due to electron accumulation in the C_{60} layer. We find that this voltage increases in the order:perovskite < perovskite|C_{60} < perovskite|SAM|C_{60}, corroborating that the incorporation of the SAM improves charge separation at the n-interface, and that the effect due to the SAM is only seen if also C_{60} is present. Therefore the main difference between the studied cells is non-radiative recombination at the perovskite/C_{60} interface, which is reduced progressively with increasing length of the SAMs.

We are able to draw the following conclusions: **1.** All four techniques (PLQY, EQE_{EL}, TRPL and SPV) are mutually in excellent agreement. **2.** The QFLS in the perovskite layer determines the V_{OC} in the devices. Therefore, all changes in V_{OC} (from the addition of the charge-transporting layers and the SAM) originate from differences in the QFLS of the absorber and must, therefore, be related to the charge recombination dynamics. Notably, the perovskite layers on glass or on the HTL both allow a V_{OC} > 1.2 V, which also means that non-radiative recombination at the interface between the perovskite and the HTL (poly-TPD) is comparably slow. **3.** The perovskite/C_{60} interface is the bottleneck for a high photovoltage output, as it reduces the obtainable V_{OC} (QFLS) to a maximum of 1.08 V (eV) on average (1.1 V max). **4.** Given that the deposition of the SAMs on the neat perovskite layer does not affect the luminescent properties or the magnitude of the SPV signal, we can rule out passivation of the perovskite surface as main reason for the shown improvement. We can, therefore, assign the improved QFLS and lifetime of the cells to suppressed across-interface recombination.

Lastly, we note that a recent similar[70] approach reports on a red-shift of the perovskite absorption onset by annealing the samples after the deposition of a similar molecule in vastly higher concentrations; while we observe essentially no change in the bandgap energy or tail-slope; see Figure S8.

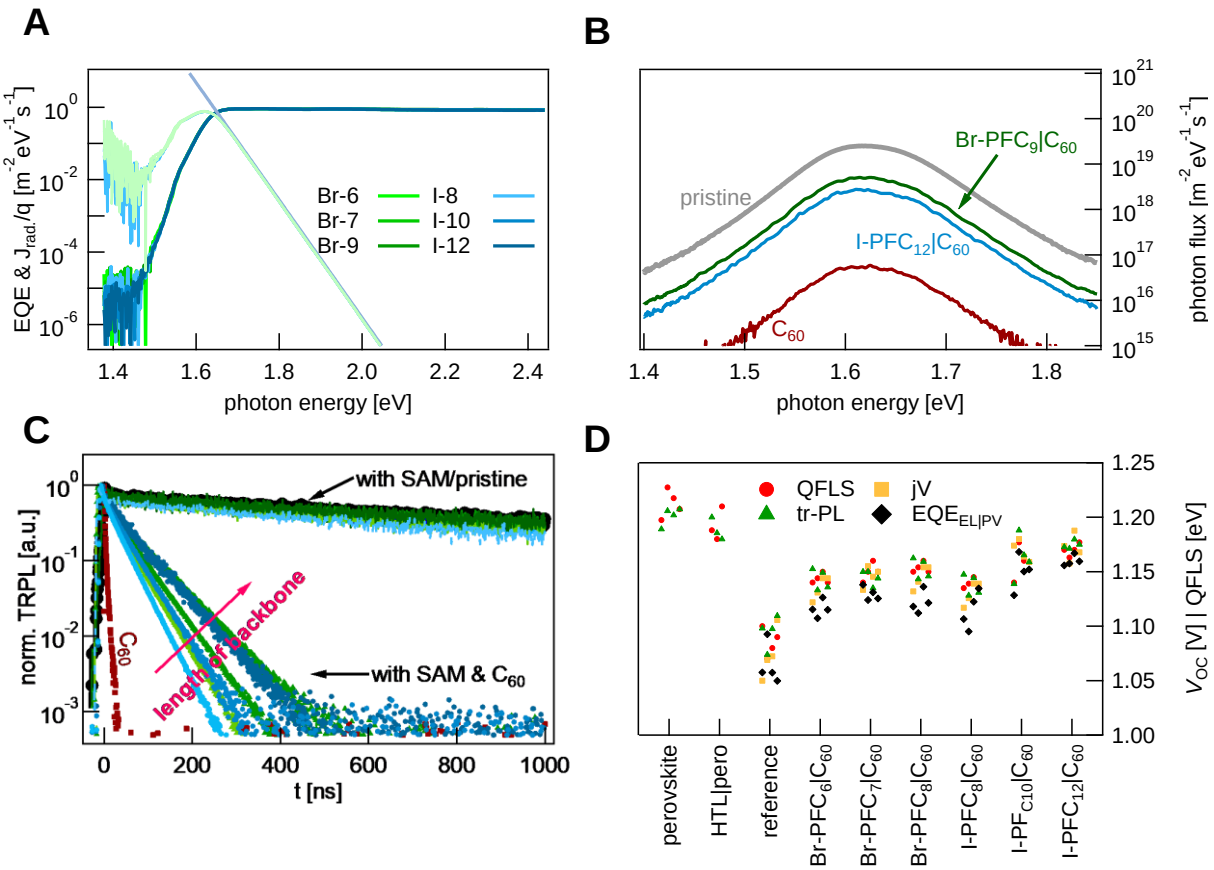

Figure 3. A) EQE_{PV} and $J_{rad.}/q$ for of the solar cells with the different interlayers. B) PL photon flux under a ~1-sun-equivalent 445 nm illumination of the neat perovskite reference, the perovskite covered with C_{60}, and with the two longest molecule chain SAMs in between. C) Normalized TRPL decays of perovskite (black dots) with the different SAMs (green and blue lines), compared to the corresponding devices with an additional C_{60} layer, with (green and blue dots) or without the SAMs (dark red dots). All measurements were performed with excitation at 470nm and ~40nJ/cm² (no~10^{15}cm^{-3}). D) Deduced QFLS or qV_{OC} as determined from the absolute PL (red), tr-PL (green), *jV* scan (yellow) or the electroluminescence efficiency (black) for several samples each.

Device Stability

Many of the state-of-the-art perovskite solar cells – irrespective of p-i-n or n-i-p architecture – show excellent performance. At the same time, the number of reports concerning enhanced stability has increased following this rapid rise in efficiency[2,3]. The general belief is that the perovskite is the weakest link in the multilayer devices. In particular the organic cations – foremost methylammonium – are blamed as the culprit due to their volatile nature. Various approaches have been employed to reduce or mitigate these losses through (partial) cation exchange with bigger molecules such as FA or GA, encapsulation, blocking layer deposition or passivation.[27,28,71–74] While most approaches concern either rigid hard encapsulation through e.g. ALD layers or additive engineering, fewer have adopted ways to improve the interfaces as a simple post-process. We sought to test the impact on stability for the best performing devices in our SAM series. We anticipated that the binding between the p-SAMs and the perovskite and the strong entanglement of the perfluorinated tail of the molecules reduces the permeability for small molecules and ions at the perovskite|C_{60} interface in either direction. As ingress of water and evolution of MA^+ are considered the Achilles heel of perovskite solar cells, preventing the latter two seems to be the natural approach. As a proof of principle, we also provide photographs of perovskite layers with a water droplet, revealing a drastic suppression of perovskite decomposition upon SAM deposition. While in the case of the untreated perovskite a yellow spot is visible shortly after dropping the water, indicating the irreversible formation of PbI_2, this irreversible decomposition is drastically slowed down in the case of I-PFC12 (both in Figure S9), where this decomposition takes

minutes to occur. This effect is likewise visible when comparing absorption spectra of a similar perovskite (slightly higher Br/I ratio) as a function of storage time in ambient conditions. In the case of a sample without functionalization, the perovskite decomposes as evident from the rise in PbI_2 absorption signal (Figure S10). We rationalize this slowdown of decomposition by measuring XRD diffractograms of perovskite films with and without I-PFC10 or Br-PFC9 after exposure to humid air (~50%RH) overnight (Figure S10D). We find that the interlayers effectively retard the ingress of water, evident from the absence of perovskite-hydrates[75] at ~11° in contrast to the unmodified perovskite (Figure S10D). This slowdown will, in turn, slow down water-induced degradation. Finally, we measured full solar cells over the course of 4 months (~3000h) both "encapsulated" in an inert atmosphere and under ambient conditions without encapsulation, with weak light exposure – i.e. shelf storage. Figure 4A shows that when stored in the inert atmosphere, both reference and modified types devices are essentially stable, while when stored in the ambient the devices without SAMs lose up to 30% of their initial (already lower) efficiency. In contrast, the devices with a modified interface retain >95% of their initial efficiency under ISOS-D-1 conditions. We conclude that surface modification effectively reduces the ingress of moisture, which we consider to be the main reason for the device degradation. The alternative to diffusion into or within the cell is the diffusion of organic cations out of the cell; especially MA+ may be lost due to this process, which potentially induces an irreversible degradation. As diffusion is a thermally activated motion, we tested the thermal stability of the individual volatile components in the perovskite. To this end, we performed differential scanning calorimetry measurements (DSC) on MAI, I-PFC10 and a combined powder (MAI + I-PFC10), as seen in Figure 4B. The melting point of pure I-PFC10 is visible at ~70°C, while MAI shows a peak at ~150°C which is associated to a phase transition of MAI from the solid crystalline phase to a pre-melting state called ionic plastic phase, as reported in literature[76,77]. In contrast, the mixed powder completely lacks the spike at 70°C and shows the same thermal transition of MAI, but is shifted by ~ 15°C to higher temperatures, indicating the stabilizing effect of I-PFC10 on MAI. These observations lead to the hypothesis, that the I-PFCx modified solar cells will be more thermally stable than the reference counterparts. We tested this hypothesis by measuring some of the most efficient devices at various relevant temperatures (Figure 4C), where we were able to extract thermal efficiency loss coefficients of -0.106%/°C and -0.122%/°C for the I-PFC10 and the reference device, indicating a small improvement in the modified cells. We note that these numbers are comparable to previous reports[78], albeit a bit lower. Finally, we subjected these cells to an intensive coupled heat-light-load stress test, by measuring the power output of the devices held at MPP at 85°C with an equivalent of ~1 sun illumination in a nitrogen atmosphere (Figure 4D), consistent with the ISOS-L-2 protocol. Much of the recent reports show normalized efficiencies, especially when performing aging tests. While we believe that in many cases this may help to visualize the improvement, we want to stress that performing standardized stress tests on the ***highest*** performing devices is essential and often omitted. Also, we explicitly did not encapsulate the devices so as to show the full potential of the SAMs.[79] Initially the cells are at room temperature and then heated within a few minutes to 85°C causing a rapid initial drop of ~ 6% absolute due to a higher thermal recombination current ($J_{rad.}$) of the device at 85°C compared to 25°C, which in turn reduces V_{OC} and V_{MPP} and thus PCE. After this, the best reference device still degraded rapidly to <5% within ~30 h. In stark contrast, the modified device recovered from the initial drop within a few hours and stabilized at 16%. This device kept this efficiency over the next 250 h without any additional loss, unprecedented in this device architecture without elaborate encapsulation strategies[27,28,80]. The high stability is highly encouraging, given the simplicity of the approach but also that the perovskite is only capped by another <40 nm of small organic molecules (C60 and BCP) and a metal cathode. We also observe a mild improvement in V_{MPP} over time (Figure S11A), which we believe is due to a light-induced modification/relaxation of the perovskite[81–83], enhancing the PLQY, which we could likewise observe for the mixed-halide/mixed-cation perovskite in a reference experiment (Figure S11B).

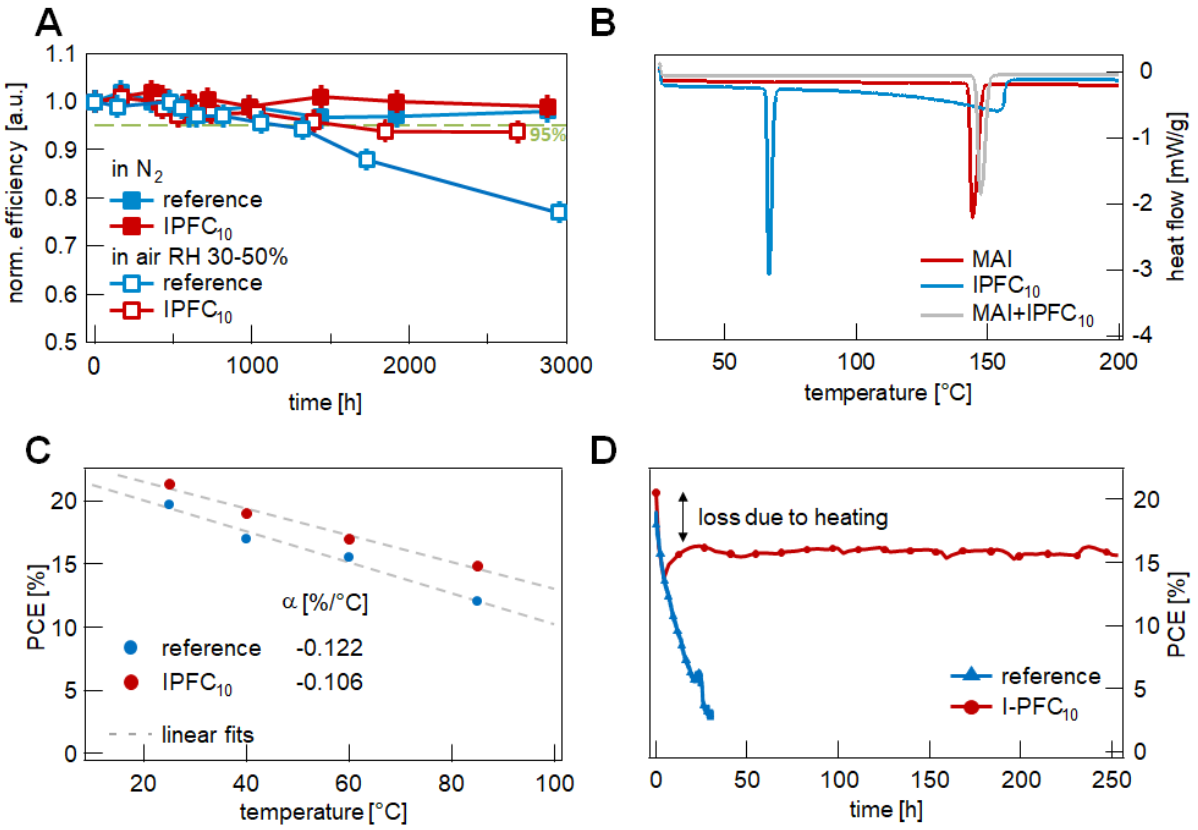

Figure 4. A) Stability of perovskite solar cells stored in nitrogen or ambient air over the course of 4 months. B) DSC measurements on MAI, I-PFC10 and a mixture of the latter, that show the interaction of the I-terminated group to iodine in MAI enhancing the latter's thermal stability. C) Temperature-dependent PCE with linear fitting renders efficiency loss coefficients of ~ 0.1%/°C. D) Maximum power point tracking at elevated temperature (85°C) in a nitrogen-filled glovebox for the reference (red) and modified device (blue). Both devices show a quick initial drop due to the increase in temperature.

Conclusion

In summary, we present a facile method to modify the perovskite absorber in highly efficient p-i-n-type solar cells through the use of perfluorinated halogenated self-assembled molecules. Functionalization of the perovskite surface with I-terminated fluorocarbons comes with a significant increase of the open-circuit voltage up to 1.18 V while leaving the other photovoltaic parameters nearly unchanged. Such SAM-functionalized perovskite devices exhibited power conversion efficiencies surpassing 21%. XPS, UPS and FTIR suggest that the SAMs interact with the perovskite surface mainly through mild electrostatic interactions. Using absolute PL, tr-PL electroluminescence and SPV measurements, we show that the deposition of the SAM has no effect on the recombination properties of the perovskite itself, ruling out trap passivation as the main reason for the performance increase. Instead, we show that the functionalization of the perovskite top surface with the fluorocarbon molecules improves charge separation and suppresses non-radiative recombination at the perovskite/C60 interface. Due to the sufficiently strong adhesion to the surface and its fluorinated water-repelling backbone, cells comprising the SAM molecules withstand harsh stress tests such as 250 h MPP-tracking at elevated temperatures (85°C) or long-term exposure to ambient air without appreciable efficiency loss under standardized harsh testing conditions (ISOS-D-1 and ISOS-L-2). This work demonstrates advancement in the quest to improve the stability and efficiency of perovskite solar cells towards industrial standards using a simple solution-based approach, without the need for elaborate and complicated processing schemes, compatible with conformal growth methods, even on rough or textured surfaces[18,19,84–86]. Combining

these dual benefits of stability and reduced interfacial recombination with surface passivation layers will be the next step towards highly efficient even more stable devices pushing this technology to the verge of commercialization.

ASSOCIATED CONTENT

Supporting Information.
Experimental Methods, Supplementary Notes and Calculations, Details on Simulation, XRD, UV-Vis, XPS, FTIR, KP data, PL vs time, SPV measurements as well as additional experimental methods.

AUTHOR INFORMATION

Corresponding Author

* Correspondence to: chriwolff@uni-potsdam.de, antonio.abate@helmholtz-berlin.de, neher@uni-potsdam.de

Author Contributions

The manuscript was written through the contributions of all authors. All authors have given approval to the final version of the manuscript.

Funding Sources

DFG – SFB951, SPP2196

Notes

Any additional relevant notes should be placed here.

ACKNOWLEDGMENT

The authors acknowledge Lab Assistance by A. Pucher, A. Horka, B. Stiller, F. Jaiser and F. Dornack (Potsdam), as well as Sandy Sanchez (Univ. Fribourg, now EPFL) for help with the DSC measurements and funding from the Helmholtz Energy Alliance "Hybrid Photovoltaics", the Potsdam Graduate School (PoGS) and HyPerCells. C. R. thanks funding from the HI-SCORE research school. Part of this work was funded by the Deutsche Forschungsgemeinschaft (DFG) under the Project ID 182087777 - SFB 951 (HIOS) and 423749265 - SPP 2196 (SURPRISE).

ABBREVIATIONS

REFERENCES

(1) Green, M. A.; Hishikawa, Y.; Dunlop, E. D.; Levi, D. H.; Hohl-Ebinger, J.; Yoshita, M.; Ho-Baillie, A. W. Y. Solar Cell Efficiency Tables (Version 53). *Prog. Photovoltaics Res. Appl.* **2019**, *27* (1), 3–12. https://doi.org/10.1002/pip.3102.

(2) Boyd, C. C.; Cheacharoen, R.; Leijtens, T.; McGehee, M. D. Understanding Degradation Mechanisms and Improving Stability of Perovskite Photovoltaics. *Chem. Rev.* **2018**, acs.chemrev.8b00336. https://doi.org/10.1021/acs.chemrev.8b00336.

(3) Christians, J. A.; Habisreutinger, S. N.; Berry, J. J.; Luther, J. M. Stability in Perovskite Photovoltaics: A Paradigm for Newfangled Technologies. *ACS Energy Lett.* **2018**, *3* (9), 2136–2143. https://doi.org/10.1021/acsenergylett.8b00914.

(4) Zhao, J.; Brinkmann, K. O.; Hu, T.; Pourdavoud, N.; Becker, T.; Gahlmann, T.; Heiderhoff, R.; Polywka, A.; Görrn, P.; Chen, Y.; et al. Self-Encapsulating Thermostable and Air-Resilient Semitransparent Perovskite Solar Cells. *Adv. Energy Mater.* **2017**, *7* (14), 1602599. https://doi.org/10.1002/aenm.201602599.

(5) Koushik, D.; Verhees, W. J. H. H.; Kuang, Y.; Veenstra, S.; Zhang, D.; Verheijen, M. A.; Creatore, M.; Schropp, R. E. I. I. High-Efficiency Humidity-Stable Planar Perovskite Solar Cells Based on Atomic Layer Architecture. *Energy Environ. Sci.* **2017**, *10* (1), 91–100. https://doi.org/10.1039/c6ee02687g.

(6) Yang, S.; Wang, Y.; Liu, P.; Cheng, Y.-B.; Zhao, H. J.; Yang, H. G. Functionalization of Perovskite Thin Films with Moisture-Tolerant Molecules. *Nat. Energy* **2016**, *1* (2), 15016. https://doi.org/10.1038/nenergy.2015.16.

(7) Li, X.; Ibrahim Dar, M.; Yi, C.; Luo, J.; Tschumi, M.; Zakeeruddin, S. M.; Nazeeruddin, M. K.; Han, H.; Grätzel, M. Improved Performance and Stability of Perovskite Solar Cells by Crystal Crosslinking with Alkylphosphonic Acid ω-Ammonium Chlorides. *Nat. Chem.* **2015**, *7* (9), 703–711. https://doi.org/10.1038/nchem.2324.

(8) Noel, N. K.; Abate, A.; Stranks, S. D.; Parrott, E. S.; Burlakov, V. M.; Goriely, A.; Snaith, H. J. Enhanced Photoluminescence and Solar Cell Performance via Lewis Base Passivation of Organic–Inorganic Lead

Halide Perovskites. *ACS Nano* **2014**, *8* (10), 9815–9821. https://doi.org/10.1021/nn5036476.
(9) Jain, S. M.; Qiu, Z.; Häggman, L.; Mirmohades, M.; Johansson, M. B.; Edvinsson, T.; Boschloo, G. Frustrated Lewis Pair-Mediated Recrystallization of CH 3 NH 3 PbI 3 for Improved Optoelectronic Quality and High Voltage Planar Perovskite Solar Cells. *Energy Environ. Sci.* **2016**, *9* (12), 3770–3782. https://doi.org/10.1039/C6EE02544G.
(10) Tsai, H.; Nie, W.; Blancon, J.-C.; Stoumpos, C. C.; Asadpour, R.; Harutyunyan, B.; Neukirch, A. J.; Verduzco, R.; Crochet, J. J.; Tretiak, S.; et al. High-Efficiency Two-Dimensional Ruddlesden–Popper Perovskite Solar Cells. *Nature* **2016**, *536* (7616), 312–316. https://doi.org/10.1038/nature18306.
(11) Grancini, G.; Roldán-Carmona, C.; Zimmermann, I.; Mosconi, E.; Lee, X.; Martineau, D.; Narbey, S.; Oswald, F.; De Angelis, F.; Graetzel, M.; et al. One-Year Stable Perovskite Solar Cells by 2D/3D Interface Engineering. *Nat. Commun.* **2017**, *8*, 15684. https://doi.org/10.1038/ncomms15684.
(12) Hu, Y.; Schlipf, J.; Wussler, M.; Petrus, M. L.; Jaegermann, W.; Bein, T.; Müller-Buschbaum, P.; Docampo, P. Hybrid Perovskite/Perovskite Heterojunction Solar Cells. *ACS Nano* **2016**, *10* (6), 5999–6007. https://doi.org/10.1021/acsnano.6b01535.
(13) Wang, Z.; Lin, Q.; Chmiel, F. P.; Sakai, N.; Herz, L. M.; Snaith, H. J. Efficient Ambient-Air-Stable Solar Cells with 2D–3D Heterostructured Butylammonium-Caesium-Formamidinium Lead Halide Perovskites. *Nat. Energy* **2017**, *2* (9), 17135. https://doi.org/10.1038/nenergy.2017.135.
(14) Christians, J. A.; Schulz, P.; Tinkham, J. S.; Schloemer, T. H.; Harvey, S. P.; Tremolet De Villers, B. J.; Sellinger, A.; Berry, J. J.; Luther, J. M. Tailored Interfaces of Unencapsulated Perovskite Solar Cells for >1,000 Hour Operational Stability. *Nat. Energy* **2018**, *3* (1), 68–74. https://doi.org/10.1038/s41560-017-0067-y.
(15) Saliba, M.; Matsui, T.; Domanski, K.; Seo, J.-Y.; Ummadisingu, A.; Zakeeruddin, S. M.; Correa-Baena, J.-P.; Tress, W. R.; Abate, A.; Hagfeldt, A.; et al. Incorporation of Rubidium Cations into Perovskite Solar Cells Improves Photovoltaic Performance. *Science* **2016**, *354* (6309), 206–209. https://doi.org/10.1126/science.aah5557.
(16) Jeon, N. J.; Na, H.; Jung, E. H.; Yang, T.-Y.; Lee, Y. G.; Kim, G.; Shin, H.-W.; Il Seok, S.; Lee, J.; Seo, J. A Fluorene-Terminated Hole-Transporting Material for Highly Efficient and Stable Perovskite Solar Cells. *Nat. Energy* **2018**, *3* (8), 682–689. https://doi.org/10.1038/s41560-018-0200-6.
(17) Wang, Q.; Phung, N.; Di Girolamo, D.; Vivo, P.; Abate, A. Enhancement in Lifespan of Halide Perovskite Solar Cells. *Energy Environ. Sci.* **2019**. https://doi.org/10.1039/C8EE02852D.
(18) Jošt, M.; Köhnen, E.; Morales-Vilches, A. B.; Lipovšek, B.; Jäger, K.; Macco, B.; Al-Ashouri, A.; Krč, J.; Korte, L.; Rech, B.; et al. Textured Interfaces in Monolithic Perovskite/Silicon Tandem Solar Cells: Advanced Light Management for Improved Efficiency and Energy Yield. *Energy Environ. Sci.* **2018**, *11* (12), 3511–3523. https://doi.org/10.1039/C8EE02469C.
(19) Sahli, F.; Werner, J.; Kamino, B. A.; Bräuninger, M.; Monnard, R.; Paviet-Salomon, B.; Barraud, L.; Ding, L.; Diaz Leon, J. J.; Sacchetto, D.; et al. Fully Textured Monolithic Perovskite/Silicon Tandem Solar Cells with 25.2% Power Conversion Efficiency. *Nat. Mater.* **2018**, *17* (9), 820–826. https://doi.org/10.1038/s41563-018-0115-4.
(20) Mazzarella, L.; Lin, Y.-H.; Kirner, S.; Morales-Vilches, A. B.; Korte, L.; Albrecht, S.; Crossland, E.; Stannowski, B.; Case, C.; Snaith, H. J.; et al. Infrared Light Management Using a Nanocrystalline Silicon Oxide Interlayer in Monolithic Perovskite/Silicon Heterojunction Tandem Solar Cells with Efficiency above 25%. *Adv. Energy Mater.* **2019**, 1803241. https://doi.org/10.1002/aenm.201803241.
(21) Luo, D.; Yang, W.; Wang, Z.; Sadhanala, A.; Hu, Q.; Su, R.; Shivanna, R.; Trindade, G. F.; Watts, J. F.; Xu, Z.; et al. Enhanced Photovoltage for Inverted Planar Heterojunction Perovskite Solar Cells. *Science* **2018**, *360* (6396), 1442–1446. https://doi.org/10.1126/science.aap9282.
(22) Wang, Q.; Dong, Q.; Li, T.; Gruverman, A.; Huang, J. Thin Insulating Tunneling Contacts for Efficient and Water-Resistant Perovskite Solar Cells. *Adv. Mater.* **2016**, *28* (31), 6734–6739. https://doi.org/10.1002/adma.201600969.
(23) Wolff, C. M.; Zu, F.; Paulke, A.; Toro, L. P.; Koch, N.; Neher, D. Reduced Interface-Mediated Recombination for High Open-Circuit Voltages in CH 3 NH 3 PbI 3 Solar Cells. *Adv. Mater.* **2017**, *29* (28), 1700159.
(24) Stolterfoht, M.; Wolff, C. M.; Márquez, J. A.; Zhang, S.; Hages, C. J.; Rothhardt, D.; Albrecht, S.; Burn, P. L.; Meredith, P.; Unold, T.; et al. Visualization and Suppression of Interfacial Recombination for High-Efficiency Large-Area Pin Perovskite Solar Cells. *Nat. Energy* **2018**, *3* (10), 847–854. https://doi.org/10.1038/s41560-018-0219-8.
(25) Zheng, X.; Chen, B.; Dai, J.; Fang, Y.; Bai, Y.; Lin, Y.; Wei, H.; Zeng, X. C. C.; Huang, J. Defect Passivation in Hybrid Perovskite Solar Cells Using Quaternary Ammonium Halide Anions and Cations. *Nat. Energy* **2017**, *2* (7), 17102. https://doi.org/10.1038/nenergy.2017.102.
(26) Stolterfoht, M.; Wolff, C. M. C. M.; Amir, Y.; Paulke, A.; Perdigón-Toro, L.; Caprioglio, P.; Neher, D. Approaching the Fill Factor Shockley–Queisser Limit in Stable, Dopant-Free Triple Cation Perovskite Solar Cells. *Energy Environ. Sci.* **2017**, *10* (6), 1530–1539. https://doi.org/10.1039/C7EE00899F.
(27) Bush, K. A.; Bailie, C. D.; Chen, Y.; Bowring, A. R.; Wang, W.; Ma, W.; Leijtens, T.; Moghadam, F.; McGehee, M. D. Thermal and Environmental Stability of Semi-Transparent Perovskite Solar Cells for Tandems Enabled by a Solution-Processed Nanoparticle Buffer Layer and Sputtered ITO Electrode. *Adv. Mater.* **2016**, *28* (20), 3937–3943. https://doi.org/10.1002/adma.201505279.
(28) Brinkmann, K. O.; Zhao, J.; Pourdavoud, N.; Becker, T.; Hu, T.; Olthof, S.; Meerholz, K.; Hoffmann, L.;

Gahlmann, T.; Heiderhoff, R.; et al. Suppressed Decomposition of Organometal Halide Perovskites by Impermeable Electron-Extraction Layers in Inverted Solar Cells. *Nat. Commun.* **2017**, *8*, 13938. https://doi.org/10.1038/ncomms13938.

(29) Bush, K. A.; Palmstrom, A. F.; Yu, Z. (Jason); Boccard, M.; Cheacharoen, R.; Mailoa, J. P.; McMeekin, D. P.; Hoye, R. L. Z.; Bailie, C. D.; Leijtens, T.; et al. 23.6%-Efficient Monolithic Perovskite/Silicon Tandem Solar Cells with Improved Stability. *Nat. Energy* **2017**, *2* (4), 17009. https://doi.org/10.1038/nenergy.2017.9.

(30) Bai, Y.; Dong, Q.; Shao, Y.; Deng, Y.; Wang, Q.; Shen, L.; Wang, D.; Wei, W.; Huang, J. Enhancing Stability and Efficiency of Perovskite Solar Cells with Crosslinkable Silane-Functionalized and Doped Fullerene. *Nat. Commun.* **2016**, *7*, 12806. https://doi.org/10.1038/ncomms12806.

(31) Seo, S.; Jeong, S.; Bae, C.; Park, N.-G.; Shin, H. Perovskite Solar Cells with Inorganic Electron- and Hole-Transport Layers Exhibiting Long-Term (≈500 h) Stability at 85 °C under Continuous 1 Sun Illumination in Ambient Air. *Adv. Mater.* **2018**, *30* (29), 1801010. https://doi.org/10.1002/adma.201801010.

(32) Calió, L.; Kazim, S.; Grätzel, M.; Ahmad, S. *Hole-Transport Materials for Perovskite Solar Cells*; John Wiley & Sons, Ltd, 2016; Vol. 55, pp 14522–14545. https://doi.org/10.1002/anie.201601757.

(33) Matsui, T.; Petrikyte, I.; Malinauskas, T.; Domanski, K.; Daskeviciene, M.; Steponaitis, M.; Gratia, P.; Tress, W.; Correa-Baena, J.-P.; Abate, A.; et al. Additive-Free Transparent Triarylamine-Based Polymeric Hole-Transport Materials for Stable Perovskite Solar Cells. *ChemSusChem* **2016**, *9* (18), 2567–2571. https://doi.org/10.1002/cssc.201600762.

(34) Guo, F.; Li, N.; Fecher, F. W.; Gasparini, N.; Quiroz, C. O. R.; Bronnbauer, C.; Hou, Y.; Radmilović, V. V.; Radmilović, V. R.; Spiecker, E.; et al. A Generic Concept to Overcome Bandgap Limitations for Designing Highly Efficient Multi-Junction Photovoltaic Cells. *Nat. Commun.* **2015**, *6*, 7730. https://doi.org/10.1038/ncomms8730.

(35) Stolterfoht, M.; Wolff, C. M.; Amir, Y.; Paulke, A.; Perdigón-Toro, L.; Caprioglio, P.; Neher, D. Approaching the Fill Factor Shockley-Queisser Limit in Stable, Dopant-Free Triple Cation Perovskite Solar Cells. *Energy Environ. Sci.* **2017**, *10* (6).

(36) Liu, Z.; Krückemeier, L.; Krogmeier, B.; Klingebiel, B.; Márquez, J. A.; Levcenko, S.; Öz, S.; Mathur, S.; Rau, U.; Unold, T.; et al. Open-Circuit Voltages Exceeding 1.26 V in Planar Methylammonium Lead Iodide Perovskite Solar Cells. *ACS Energy Lett.* **2018**, 110–117. https://doi.org/10.1021/acsenergylett.8b01906.

(37) Abate, A.; Saliba, M.; Hollman, D. J.; Stranks, S. D.; Wojciechowski, K.; Avolio, R.; Grancini, G.; Petrozza, A.; Snaith, H. J. Supramolecular Halogen Bond Passivation of Organic–Inorganic Halide Perovskite Solar Cells. *Nano Lett.* **2014**, *14* (6), 3247–3254. https://doi.org/10.1021/nl500627x.

(38) Abate, A.; Dehmel, R.; Sepe, A.; Nguyen, N. L.; Roose, B.; Marzari, N.; Hong, J. K.; Hook, J. M.; Steiner, U.; Neto, C. Halogen-Bond Driven Self-Assembly of Perfluorocarbon Monolayers on Silicon Nitride. *J. Mater. Chem. A* **2019**, *7* (42), 24445–24453. https://doi.org/10.1039/C9TA04620H.

(39) Leblebici, S. Y.; Leppert, L.; Li, Y.; Reyes-Lillo, S. E.; Wickenburg, S.; Wong, E.; Lee, J.; Melli, M.; Ziegler, D.; Angell, D. K.; et al. Facet-Dependent Photovoltaic Efficiency Variations in Single Grains of Hybrid Halide Perovskite. *Nat. Energy* **2016**, *1* (8), 16093. https://doi.org/10.1038/nenergy.2016.93.

(40) Abate, A.; Dehmel, R.; Sepe, A.; Nguyen, N. L.; Roose, B.; Marzari, N.; Hong, J. K.; Hook, J. M.; Steiner, U.; Neto, C. Halogen-Bond Driven Self-Assembly of Perfluorocarbon Monolayers. *arXiv.org* **2018**. https://doi.org/arXiv:1803.05672.

(41) Löwdin, P. On the Non-Orthogonality Problem Connected with the Use of Atomic Wave Functions in the Theory of Molecules and Crystals. *J. Chem. Phys.* **1950**, *18* (3), 365–375. https://doi.org/10.1063/1.1747632.

(42) Monkhorst, H. J.; Pack, J. D. Special Points for Brillouin-Zone Integrations. *Phys. Rev. B* **1976**, *13* (12), 5188–5192. https://doi.org/10.1103/PhysRevB.13.5188.

(43) Perdew, J. P.; Burke, K.; Ernzerhof, M. Generalized Gradient Approximation Made Simple. *Phys. Rev. Lett.* **1996**, *77* (18), 3865–3868. https://doi.org/10.1103/PhysRevLett.77.3865.

(44) Giannozzi, P.; Baroni, S.; Bonini, N.; Calandra, M.; Car, R.; Cavazzoni, C.; Ceresoli, D.; Chiarotti, G. L.; Cococcioni, M.; Dabo, I.; et al. QUANTUM ESPRESSO: A Modular and Open-Source Software Project for Quantum Simulations of Materials. *J. Phys. Condens. Matter* **2009**, *21* (39), 395502. https://doi.org/10.1088/0953-8984/21/39/395502.

(45) Sabatini, R.; Gorni, T.; de Gironcoli, S. Nonlocal van Der Waals Density Functional Made Simple and Efficient. *Phys. Rev. B* **2013**, *87* (4), 041108. https://doi.org/10.1103/PhysRevB.87.041108.

(46) Clark, T.; Hennemann, M.; Murray, J. S.; Politzer, P. Halogen Bonding: The σ-Hole: Proceedings of "Modeling Interactions in Biomolecules II", Prague, September 5th-9th, 2005. *J. Mol. Model.* **2007**, *13* (2), 291–296. https://doi.org/10.1007/s00894-006-0130-2.

(47) Cavallo, G.; Metrangolo, P.; Milani, R.; Pilati, T.; Priimagi, A.; Resnati, G.; Terraneo, G. The Halogen Bond. *Chemical Reviews*. American Chemical Society February 24, 2016, pp 2478–2601. https://doi.org/10.1021/acs.chemrev.5b00484.

(48) Schondelmaier, D.; Cramm, S.; Klingeler, R.; Morenzin, J.; Zilkens, C.; Eberhardt, W. Orientation and Self-Assembly of Hydrophobic Fluoroalkylsilanes. *Langmuir* **2002**, *18* (16), 6242–6245. https://doi.org/10.1021/la0256533.

(49) Shou, K.; Hong, J. K.; Wood, E. S.; Hook, J. M.; Nelson, A.; Yin, Y.; Andersson, G. G.; Abate, A.; Steiner, U.; Neto, C. Ultralow Surface Energy Self-Assembled Monolayers of Iodo-Perfluorinated Alkanes on Silica Driven by Halogen Bonding. *Nanoscale* **2019**, *11* (5), 2401–2411. https://doi.org/10.1039/c8nr08195f.

(50) Tvingstedt, K.; Gil-Escrig, L.; Momblona, C.; Rieder, P.; Kiermasch, D.; Sessolo, M.; Baumann, A.; Bolink, H. J.; Dyakonov, V. Removing Leakage and Surface Recombination in Planar Perovskite Solar Cells. *ACS Energy Lett.* **2017**, *2* (2), 424–430. https://doi.org/10.1021/acsenergylett.6b00719.

(51) Kiermasch, D.; Rieder, P.; Tvingstedt, K.; Baumann, A.; Dyakonov, V. Improved Charge Carrier Lifetime in Planar Perovskite Solar Cells by Bromine Doping. *Sci. Rep.* **2016**, *6* (1), 39333. https://doi.org/10.1038/srep39333.

(52) Tvingstedt, K.; Malinkiewicz, O.; Baumann, A.; Deibel, C.; Snaith, H. J.; Dyakonov, V.; Bolink, H. J. Radiative Efficiency of Lead Iodide Based Perovskite Solar Cells. *Sci. Rep.* **2014**, *4*, 6071. https://doi.org/10.1038/srep06071.

(53) Bi, D.; Tress, W.; Dar, M. I.; Gao, P.; Luo, J.; Renevier, C.; Schenk, K.; Abate, A.; Giordano, F.; Correa Baena, J.-P.; et al. Efficient Luminescent Solar Cells Based on Tailored Mixed-Cation Perovskites. *Sci. Adv.* **2016**, *2* (1).

(54) Correa-Baena, J.-P.; Tress, W.; Domanski, K.; Anaraki, E. H.; Turren-Cruz, S.-H.; Roose, B.; Boix, P. P.; Grätzel, M.; Saliba, M.; Abate, A.; et al. Identifying and Suppressing Interfacial Recombination to Achieve High Open-Circuit Voltage in Perovskite Solar Cells. *Energy Environ. Sci.* **2017**, *10* (5), 1207–1212. https://doi.org/10.1039/C7EE00421D.

(55) Caprioglio, P.; Zu, F.; Wolff, C. M.; Márquez Prieto, J. A.; Stolterfoht, M.; Becker, P.; Koch, N.; Unold, T.; Rech, B.; Albrecht, S.; et al. High Open Circuit Voltages in Pin-Type Perovskite Solar Cells through Strontium Addition. *Sustain. Energy Fuels* **2019**, *3* (2), 550–563. https://doi.org/10.1039/C8SE00509E.

(56) Cai, B.; Peng, Y.; Cheng, Y.; Gu, M. 4-Fold Photocurrent Enhancement in Ultrathin Nanoplasmonic Perovskite Solar Cells. *Opt. Express* **2015**, *23* (24), A1700. https://doi.org/10.1364/OE.23.0A1700.

(57) Peng, J.; Khan, J. I.; Liu, W.; Ugur, E.; Duong, T.; Wu, Y.; Shen, H.; Wang, K.; Dang, H.; Aydin, E.; et al. A Universal Double-Side Passivation for High Open-Circuit Voltage in Perovskite Solar Cells: Role of Carbonyl Groups in Poly(Methyl Methacrylate). *Adv. Energy Mater.* **2018**, *8* (30), 1801208. https://doi.org/10.1002/aenm.201801208.

(58) Stolterfoht, M.; Caprioglio, P.; Wolff, C. M.; Márquez, J. A.; Nordmann, J.; Zhang, S.; Rothhart, D.; Hörmann, U.; Redinger, A.; Kegelmann, L.; et al. The Perovskite/Transport Layer Interfaces Dominate Non-Radiative Recombination in Efficient Perovskite Solar Cells. *arXiv.org* **2018**.

(59) Unold, T.; Gütay, L. Photoluminescence Analysis of Thin-Film Solar Cells. In *Advanced Characterization Techniques for Thin Film Solar Cells*; Wiley-VCH Verlag GmbH & Co. KGaA: Weinheim, Germany, 2016; pp 275–297. https://doi.org/10.1002/9783527699025.ch11.

(60) Wright, A. D.; Verdi, C.; Milot, R. L.; Eperon, G. E.; Pérez-Osorio, M. A.; Snaith, H. J.; Giustino, F.; Johnston, M. B.; Herz, L. M. Electron–Phonon Coupling in Hybrid Lead Halide Perovskites. *Nat. Commun.* **2016**, *7*, 11755. https://doi.org/10.1038/ncomms11755.

(61) Stranks, S. D. Nonradiative Losses in Metal Halide Perovskites. *ACS Energy Lett.* **2017**, *2* (7), 1515–1525. https://doi.org/10.1021/acsenergylett.7b00239.

(62) Rau, U. Reciprocity Relation between Photovoltaic Quantum Efficiency and Electroluminescent Emission of Solar Cells. *Phys. Rev. B* **2007**, *76* (8), 085303. https://doi.org/10.1103/PhysRevB.76.085303.

(63) Staub, F.; Hempel, H.; Hebig, J.-C.; Mock, J.; Paetzold, U. W.; Rau, U.; Unold, T.; Kirchartz, T. Beyond Bulk Lifetimes: Insights into Lead Halide Perovskite Films from Time-Resolved Photoluminescence. *Phys. Rev. Appl.* **2016**, *6* (4), 044017. https://doi.org/10.1103/PhysRevApplied.6.044017.

(64) Tress, W. Perovskite Solar Cells on the Way to Their Radiative Efficiency Limit - Insights Into a Success Story of High Open-Circuit Voltage and Low Recombination. *Adv. Energy Mater.* **2017**, *7* (14), 1602358. https://doi.org/10.1002/aenm.201602358.

(65) Kiermasch, D.; Baumann, A.; Fischer, M.; Dyakonov, V.; Tvingstedt, K. Revisiting Lifetimes from Transient Electrical Characterization of Thin Film Solar Cells; a Capacitive Concern Evaluated for Silicon, Organic and Perovskite Devices. *Energy Environ. Sci.* **2018**, *11* (3), 629–640. https://doi.org/10.1039/C7EE03155F.

(66) Richter, J. M.; Abdi-Jalebi, M.; Sadhanala, A.; Tabachnyk, M.; Rivett, J. P. H.; Pazos-Outón, L. M.; Gödel, K. C.; Price, M.; Deschler, F.; Friend, R. H. Enhancing Photoluminescence Yields in Lead Halide Perovskites by Photon Recycling and Light Out-Coupling. *Nat. Commun.* **2016**, *7*, 13941. https://doi.org/10.1038/ncomms13941.

(67) Xing, Y.; Sun, C.; Yip, H. L.; Bazan, G. C.; Huang, F.; Cao, Y. New Fullerene Design Enables Efficient Passivation of Surface Traps in High Performance P-i-n Heterojunction Perovskite Solar Cells. *Nano Energy* **2016**, *26*, 7–15. https://doi.org/10.1016/j.nanoen.2016.04.057.

(68) Shih, Y. C.; Wang, L.; Hsieh, H. C.; Lin, K. F. Effect of Fullerene Passivation on the Charging and Discharging Behavior of Perovskite Solar Cells: Reduction of Bound Charges and Ion Accumulation. *ACS Appl. Mater. Interfaces* **2018**, *10* (14), 11722–11731. https://doi.org/10.1021/acsami.8b03116.

(69) Kirchartz, T.; Nelson, J.; Rau, U. Reciprocity between Charge Injection and Extraction and Its Influence on the Interpretation of Electroluminescence Spectra in Organic Solar Cells. *Phys. Rev. Appl.* **2016**, *5* (5), 054003. https://doi.org/10.1103/PhysRevApplied.5.054003.

(70) Salim, K. M. M.; Koh, T. M.; Bahulayan, D.; Harikesh, P. C.; Jamaludin, N. F.; Febriansyah, B.; Bruno, A.; Mhaisalkar, S.; Mathews, N. Extended Absorption Window and Improved Stability of Cesium-Based Triple-Cation Perovskite Solar Cells Passivated with Perfluorinated Organics. *ACS Energy Lett.* **2018**, *3* (5), 1068–1076. https://doi.org/10.1021/acsenergylett.8b00328.

(71) Turren-Cruz, S.-H.; Hagfeldt, A.; Saliba, M. Methylammonium-Free, High-Performance and Stable Perovskite Solar Cells on a Planar Architecture. *Science* **2018**, *362* (6413), eaat3583. https://doi.org/10.1126/science.aat3583.

(72) Cheacharoen, R.; Rolston, N.; Harwood, D.; Bush, K. A.; Dauskardt, R. H.; McGehee, M. D. Design and Understanding of Encapsulated Perovskite Solar Cells to Withstand Temperature Cycling. *Energy Environ. Sci.* **2018**. https://doi.org/10.1039/C7EE02564E.

(73) Ramos, F. J.; Maindron, T.; Béchu, S.; Rebai, A.; Frégnaux, M.; Bouttemy, M.; Rousset, J.; Schulz, P.; Schneider, N. Versatile Perovskite Solar Cell Encapsulation by Low-Temperature ALD-Al $_2$ O $_3$ with Long-Term Stability Improvement. *Sustain. Energy Fuels* **2018**, *2* (11), 2468–2479. https://doi.org/10.1039/C8SE00282G.

(74) Jodlowski, A. D.; Roldán-Carmona, C.; Grancini, G.; Salado, M.; Ralaiarisoa, M.; Ahmad, S.; Koch, N.; Camacho, L.; de Miguel, G.; Nazeeruddin, M. K. Large Guanidinium Cation Mixed with Methylammonium in Lead Iodide Perovskites for 19% Efficient Solar Cells. *Nat. Energy* **2017**, *2* (12), 972–979. https://doi.org/10.1038/s41560-017-0054-3.

(75) Leguy, A. M. A.; Hu, Y.; Campoy-Quiles, M.; Alonso, M. I.; Weber, O. J.; Azarhoosh, P.; Van Schilfgaarde, M.; Weller, M. T.; Bein, T.; Nelson, J.; et al. Reversible Hydration of CH<inf>3</Inf>NH<inf>3</Inf>PbI<inf>3</Inf> in Films, Single Crystals, and Solar Cells. *Chem. Mater.* **2015**, *27* (9), 3397–3407. https://doi.org/10.1021/acs.chemmater.5b00660.

(76) Ishida, H.; Ikeda, R.; Nakamura, D. Pre-Melting State of Methylammonium Iodide as Revealed by Proton Magnetic Resonance. *Phys. status solidi* **1982**, *70* (2), K151–K154. https://doi.org/10.1002/pssa.2210700261.

(77) Song, Z.; Watthage, S. C.; Phillips, A. B.; Tompkins, B. L.; Ellingson, R. J.; Heben, M. J. Impact of Processing Temperature and Composition on the Formation of Methylammonium Lead Iodide Perovskites. *Chem. Mater.* **2015**, *27* (13), 4612–4619. https://doi.org/10.1021/acs.chemmater.5b01017.

(78) Fu, F.; Feurer, T.; Weiss, T. P. P.; Pisoni, S.; Avancini, E.; Andres, C.; Buecheler, S.; Tiwari, A. N. N. High-Efficiency Inverted Semi-Transparent Planar Perovskite Solar Cells in Substrate Configuration. *Nat. Energy* **2017**, *2* (1), 16190. https://doi.org/10.1038/nenergy.2016.190.

(79) Domanski, K.; Alharbi, E. A.; Hagfeldt, A.; Grätzel, M.; Tress, W. Systematic Investigation of the Impact of Operation Conditions on the Degradation Behaviour of Perovskite Solar Cells. *Nat. Energy* **2018**, *3* (1), 61–67. https://doi.org/10.1038/s41560-017-0060-5.

(80) Zhu, Z.; Bai, Y.; Liu, X.; Chueh, C.-C.; Yang, S.; Jen, A. K.-Y. Enhanced Efficiency and Stability of Inverted Perovskite Solar Cells Using Highly Crystalline SnO $_2$ Nanocrystals as the Robust Electron-Transporting Layer. *Adv. Mater.* **2016**, *28* (30), 6478–6484. https://doi.org/10.1002/adma.201600619.

(81) Tsai, H.; Asadpour, R.; Blancon, J.-C.; Stoumpos, C. C.; Durand, O.; Strzalka, J. W.; Chen, B.; Verduzco, R.; Ajayan, P. M.; Tretiak, S.; et al. Light-Induced Lattice Expansion Leads to High-Efficiency Perovskite Solar Cells. *Science* **2018**, *360* (6384), 67–70. https://doi.org/10.1126/science.aap8671.

(82) Stavrakas, C.; Zhumekenov, A. A.; Brenes, R.; Abdi-Jalebi, M.; Bulović, V.; Bakr, O. M.; Barnard, E. S.; Stranks, S. D. Probing Buried Recombination Pathways in Perovskite Structures Using 3D Photoluminescence Tomography. *Energy Environ. Sci.* **2018**, *11* (10), 2846–2852. https://doi.org/10.1039/C8EE00928G.

(83) Brenes, R.; Guo, D.; Osherov, A.; Noel, N. K.; Eames, C.; Hutter, E. M.; Pathak, S. K.; Niroui, F.; Friend, R. H.; Islam, M. S.; et al. Metal Halide Perovskite Polycrystalline Films Exhibiting Properties of Single Crystals. *Joule* **2017**, *1* (1), 155–167. https://doi.org/10.1016/j.joule.2017.08.006.

(84) Werner, J.; Sahli, F.; Fu, F.; Diaz Leon, J. J.; Walter, A.; Kamino, B. A.; Niesen, B.; Nicolay, S.; Jeangros, Q.; Ballif, C. Perovskite/Perovskite/Silicon Monolithic Triple-Junction Solar Cells with a Fully Textured Design. *ACS Energy Lett.* **2018**, *3* (9), 2052–2058. https://doi.org/10.1021/acsenergylett.8b01165.

(85) Al-Ashouri, A.; Magomedov, A.; Roß, M.; Jošt, M.; Talaikis, M.; Chistiakova, G.; Bertram, T.; Márquez, J. A.; Köhnen, E.; Kasparavičius, E.; et al. Conformal Monolayer Contacts with Lossless Interfaces for Perovskite Single Junction and Monolithic Tandem Solar Cells. *Energy Environ. Sci.* **2019**. https://doi.org/10.1039/C9EE02268F.

(86) Jošt, M.; Bertram, T.; Koushik, D.; Marquez, J. A.; Verheijen, M. A.; Heinemann, M. D.; Köhnen, E.; Al-Ashouri, A.; Braunger, S.; Lang, F.; et al. 21.6%-Efficient Monolithic Perovskite/Cu(In,Ga)Se $_2$ Tandem Solar Cells with Thin Conformal Hole Transport Layers for Integration on Rough Bottom Cell Surfaces. *ACS Energy Lett.* **2019**, *4* (2), 583–590. https://doi.org/10.1021/acsenergylett.9b00135.